

Article

Optimal Global Positioning System/European Geostationary Navigation Overlay Service Positioning Model Using Smartphone

Grzegorz Grunwald ^{1,*}, Adam Ciećko ¹, Kamil Krasuski ² and Dariusz Tanajewski ³

¹ Faculty of Geoengineering, University of Warmia and Mazury in Olsztyn, 10-720 Olsztyn, Poland; a.ciecko@uwm.edu.pl

² Institute of Navigation, Military University of Aviation, 08-521 Dęblin, Poland; k.krasuski@law.mil.pl

³ Four Point, 51-162 Wrocław, Poland; dariusz.tanajewski@fourpoint.space

* Correspondence: grzegorz.grunwald@uwm.edu.pl

Abstract: The potential for the use of smartphones in GNSSs (Global Navigation Satellite Systems) positioning has increased in recent years due to the emergence of the ability of Android-based devices used to process raw satellite data. This paper presents the results of a study on the use of SBAS data transmitted by the EGNOS (European Geostationary Navigation Overlay Service) system in GNSS positioning using a Xiaomi Mi8 smartphone. Raw data recorded at a fixed point were used in post-processing calculations in GPS/EGNOS positioning by determining the coordinates for every second of a session of about 5 h and comparing the results to those obtained with a Septentrio AsteRx2 GNSS receiver operating at the same time at a distance of about 3 m. The calculations were performed using the assumptions of the GNSS/SBAS positioning algorithms, which were modified with carrier-phase smoothed code observations and the content of the corrections transmitted by EGNOS.

Keywords: GPS/EGNOS; Satellite-Based Augmentation System (SBAS); smartphone positioning



Citation: Grunwald, G.; Ciećko, A.; Krasuski, K.; Tanajewski, D. Optimal Global Positioning System/European Geostationary Navigation Overlay Service Positioning Model Using Smartphone. *Appl. Sci.* **2024**, *14*, 1840. <https://doi.org/10.3390/app14051840>

Academic Editor: Alessandro Lo Schiavo

Received: 25 January 2024

Revised: 19 February 2024

Accepted: 20 February 2024

Published: 23 February 2024



Copyright: © 2024 by the authors. Licensee MDPI, Basel, Switzerland. This article is an open access article distributed under the terms and conditions of the Creative Commons Attribution (CC BY) license (<https://creativecommons.org/licenses/by/4.0/>).

1. Introduction

The main purpose of SBASs (Satellite-Based Augmentation Systems) is to support civil aviation tasks. However, due to their ability to improve the quality parameters of GNSS positioning, they can also have other applications [1–4]. The operation of SBAS systems relies on the use of geostationary satellites to transmit correction data and other information that can improve GNSS positioning. EGNOS is a European system based on the transmission of data using three geostationary satellites. In addition to EGNOS, the main SBAS group includes the US WAAS (Wide Area Augmentation System), Russia's SDCM (System of Differential Correction and Monitoring), Japan's MSAS (Multi-functional Satellite Augmentation System), India's GAGAN (GPS-Aided Geosynchronous Augmented Navigation System), China's Beidou SBAS BDSBAS, and Australia's SouthPAN (Southern Positioning Augmentation Network) [5]. With real-time transmitted data, EGNOS can significantly improve the accuracy of autonomous positioning using code-based observations [6–8]. Depending on the observation conditions and measurement equipment, real-time accuracy of several tens of centimetres can be achieved. In [9], EGNOS was used to integrate a measurement system with INS (Inertial Navigation System) for autonomous ships in Inland Waterways. In turn, Ref. [10] investigated the impact of using EGNOS for Remotely Piloted Aircraft System (RPAS) positioning.

In 2016, a smartphone with the ability to record raw GNSS data using the Android Nougat operating system was made available for the first time [11,12]. Over time, the capabilities were increased in terms of the types of observations that could be recorded, starting with GPS data at L1 frequency. In 2018, a Xiaomi Mi8 smartphone running on the Broadcom BCM47755 GNSS chipset was made available to users, characterised by the

ability to record full GNSS observations including L5 GPS, QZSS frequencies, and E5a Galileo [13,14]. Today, many mobile devices offer similar capabilities.

A significant problem with recording raw GNSS data with smartphones is duty cycling, which is a process during which the smartphone's chipset runs in discontinuous mode. This results in a saving in battery consumption, but at the same time activates cycle slips during positioning. In paper [15], the results of the effect of duty cycling on GNSS code and phase observations were presented. Currently offered Android-based mobile devices are very often not using duty cycling, as is the case for the Xiaomi Mi8.

The ability of smartphones to record raw GNSS data has led to a great number of application uses. The paper [16] presents the use of raw GNSS data acquired with a smartphone for geophysical applications. The paper [17] presents the possibilities of using raw GNSS data in SPP (single-point positioning) and PPP (precise point positioning) using a smartphone. Raw satellite observations acquired with a smartphone are also being investigated for new concepts in RTK (real-time kinematic) positioning technology [18], as well as anti-spoofing and anti-jamming solutions [19].

The paper [20] presents the results of horizontal single-point positioning for smartphone measurements based on raw GNSS data and frequency E5. The root mean square error of these measurements was at the level of 4.57 m. The paper [21] presents the results of a multi-GNSS single-frequency (L1/E1/B1/G1) positioning solution obtained by Huawei P30 with a horizontal RMS of 3.24 m. On the other hand, the use of raw GNSS data on smartphones for DGNSS positioning can yield accuracy results of 1.5 m [22].

According to [23], by augmenting smartphone positioning with EGNOS and DGNSS corrections, it is possible to obtain a horizontal accuracy of better than 1 m with 95% availability. In [24], the possibility of SBAS single-frequency multiple-constellation positioning using raw GNSS data acquired with a smartphone was investigated obtaining a horizontal RMS of 1.30 m and a vertical RMS of 2.06 m. The use of smartphones in GNSS/SBAS positioning could have interesting results using DFMC (dual-frequency multi-constellation SBAS). It is envisaged that DFMC will be able to support SBAS positioning with four GNSS systems by 2025 [25–27].

The motivation for this article is the dynamic development of applications related to the use of raw GNSS data acquired with smartphones. Given the limitations on the amount and type of data that can be processed by smartphones, we decided to see how modifications to the basic GPS/EGNOS algorithm could possibly improve autonomous positioning. The aim of this paper is to investigate the feasibility of a modified satellite positioning algorithm using a smartphone and data associated with GPS and EGNOS. During the calculations, the effects of carrier-phase smoothed code observations, correction components determined using EGNOS, and modifying the observation weighting model were analysed.

The remainder of the article presents the research methodology and related issues, followed by the results of the fieldwork and conclusions.

2. Materials and Methods

Positioning using SBAS is achieved by implementing corrections to the mathematical model of positioning. In SBAS systems, data related to long-term correction, fast correction, ionospheric delay and tropospheric delay, among others, are transmitted to improve positioning quality. The corrected pseudorange determined in SBAS systems can be written with the general formula [28,29]:

$$P_{corr} = P_{meas} + RC_{fast} + RC_{clock} - RC_{iono} + RC_{tropo} \quad (1)$$

where

P_{corr} is the corrected pseudorange based on SBAS data;

P_{meas} is the pseudorange as measured by the receiver;

RC_{fast} is the fast correction;

RC_{clock} is the clock correction;

RC_{iono} is the ionospheric correction;

RC_{tropo} is the tropospheric correction.

Short-term corrections are used to correct rapid changes in ephemeris errors and clock errors [30]. They are applied in all positioning modes of air operations using SBAS with an interval of no more than 60 s. Fast corrections for a given epoch can be calculated according to the formula:

$$RC_{fast}(t) = PRC(1) + RRC(t_1)(t - t_1) \tag{2}$$

where

RC_{fast} is the total fast correction,

PRC is the pseudorange correction,

RRC is the range rate correction,

t is the user time,

t_1 is the application time of the most up-to-date fast correction.

Range rate corrections are not transmitted by SBAS systems, but calculated at receiver algorithm level:

$$RRC(t_1) = \frac{PRC(t_1) - PRC(t_0)}{t_1 - t_0} \tag{3}$$

where

t_0 is the time of application of the recently received fast correction.

The use of raw GNSS data in smartphone-based positioning puts some strain on the computing resources of Android-based devices. The use of fast corrections in the GNSS receiver algorithm significantly consumes the bandwidth of transmitted messages [24].

Long-term corrections are used to correct infrequent changes in ephemeris errors and clock errors of GPS satellites [30]. Data on the parameters of the satellites' orbits and information on the coefficients are transmitted to determine the values of the clock corrections. Some of the correction data are applied to the calculated satellite positions and velocity, while the remaining data are applied to the pseudorange measurements. Corrections to satellite positions are calculated using linear interpolation and applied to satellite positions according to the following formulas:

$$DX(t) = DX + DX_{ROC}(t - t_V) \tag{4}$$

$$DY(t) = DY + DY_{ROC}(t - t_V) \tag{5}$$

$$DZ(t) = DZ + DZ_{ROC}(t - t_V) \tag{6}$$

where

$DX(t), DY(t), DZ(t)$ are the current corrections for satellite position;

DX, DY, DZ are the corrections to satellite positions transmitted as part of slow corrections;

$DX_{ROC}, DY_{ROC}, DZ_{ROC}$ are transmitted adjustments to velocity;

t is the user time;

t_V is the application time of transmitted corrections to velocity.

Slow corrections related to satellite clocks are determined by the following formula:

$$RC_{clock} = [\delta a_{f0} + \delta a_{f1}(t - t_0)]c \tag{7}$$

where

RC_{clock} is the resulting correction of the satellite clock;

$\delta a_{f0}, \delta a_{f1}$ are clock correction parameters provided in EGNOS system messages;

t is the user time;

t_0 is the time of application of clock correction parameters;

c is the speed of propagation of an electromagnetic wave in a vacuum.

Standard satellite clock corrections determined for absolute GNSS positioning and additional clock corrections determined based on the SBAS model are calculated independently. Applying them to GNSS/SBAS positioning is also carried out independently.

The impact of the ionospheric correction on GNSS/SBAS positioning has been the subject of many scientific studies [31–36]. According to [30], its value is determined by either an SBAS model or a classical model based on the Klobuchar algorithm. Scientific publications show better positioning results when using a model based on data transmitted by EGNOS.

The ionospheric slant delay RC_{iono} determined according to the model used in EGNOS (based on four-point interpolation), can be determined by the following formula [30]:

$$RC_{iono} = -F_{pp}\tau_{vpp}(\lambda_{pp}, \phi_{pp}) \tag{8}$$

where

F_{pp} is a coefficient that changes vertical delay to slant;

τ_{vpp} is the vertical ionospheric delay for IPP;

λ_{pp}, ϕ_{pp} are IPP coordinates.

F_{pp} and τ_{vpp} can be determined from the following formulae:

$$F_{pp} = \left[1 - \left(\frac{R_e \cos E}{R_e + h_I} \right)^2 \right]^{-\frac{1}{2}} \tag{9}$$

$$\tau_{vpp} = \sum_{i=1}^4 W_i(x_{pp}, y_{pp}) \tau_{vi} \tag{10}$$

where

R_e is the Earth’s radius;

E is the elevation of the satellite;

h_I is the altitude at which the highest electron density occurs (350 km);

τ_{vi} are vertical delays for four gridpoints, transmitted by EGNOS;

$W_i(x_{pp}, y_{pp})$ is the weighing function.

SBAS systems use averaged and seasonal atmospheric data determined for a specific day and user position to determine the tropospheric correction. The model is based on tropospheric delay values towards the zenith, determined based on five meteorological parameters: pressure, temperature, water vapour pressure, rate of change of temperature, and rate of change of water vapour pressure. Their values are made available from meteorological data mainly from North American centres.

The influence of tropospheric refraction on GPS/EGNOS positioning results is determined individually for the receiver location (without using EGNOS transmitted data).

According to [30], the tropospheric delay TC_i for satellite i takes the following form:

$$TC_i = -\left(d_{hyd} + d_{wet} \right) \cdot m(El_i) \tag{11}$$

where

d_{hyd}, d_{wet} (m) are estimated signal delays for a satellite at zenith, determined from receiver altitude, pressure, temperature, water vapour pressure, rate of change of temperature, and rate of change of water vapour pressure,

$m(El_i)$ is the mapping function that transforms the delay based on the satellite’s current horizontal altitude (El_i).

Previous studies on the quality of the tropospheric EGNOS model have shown very good correlation with the Saastamoinen model, which is considered to accurately represent the local state of the troposphere [37].

The use of smoothing according to the Hutch filter of carrier-phase smoothed code observations in GPS/EGNOS positioning before applying EGNOS corrections can reduce the noise level [30,38]:

$$PR_k^S = \alpha PR_{k-1}^C + (1 - \alpha) \left[PR_{k-1}^P + \frac{\lambda}{2\pi} (PR_k^P - PR_{k-1}^P) \right] \quad (12)$$

$$\alpha = \frac{dt}{T} \quad (13)$$

where

PR_k^S is the smoothed pseudorange code;

PR_{k-1}^C is the code pseudorange in the epoch k ;

PR_k^P is the pseudorange distance in the epoch k ;

λ is the wavelength of GPS carrier frequency at L_1 ;

T is the smoothing constant;

dt is the sampling interval.

Data acquired with a Xiaomi Mi 8 smartphone (Xiaomi Corporation, Beijing, China) operating in duty cycling off mode were used for the study. Satellite observations were recorded on 25 April 2020 between 7:00 and 12:00 GPS time with an interval of 1 s in the vicinity of the city of Olsztyn in the north-eastern part of Poland. Measurements were taken at a fixed point over which a Xiaomi Mi8 smartphone was mounted on a tripod. At a distance of approximately 3 m, data were collected simultaneously using a Septentrio AsteRx2 receiver (Septentrio, Leuven, Belgium), which was equipped with a geodesic-grade antenna that has a uniform quasi-hemispherical gain pattern, right-handed circular polarisation, and a stable phase centre (Figure 1). The collected raw observational data were computed in gLAB v5.5.0 software and using proprietary computational scripts [39,40].



Figure 1. Xiaomi Mi8 smartphone (right) and Septentrio AsteRx2 receiver (left) during the measurement.

In the first stage of development, GPS/EGNOS positions were determined in post-processing mode by modifying the assumptions related to the carrier-phase smoothing of code observations. The official recommendations of the Minimum Operational Performance Standards assume that a satellite of any GNSS system can be included in the calculation if it has reached a steady state, i.e., if code observations from that satellite have been smoothed by carrier-phase observations for at least 6 min. The smoothing window associated with smoothing observations is defined as the product of the number of samples accepted for the calculation and the interval of the measurement data. This is related to restrictive aviation applications, which may not translate into validity for use in smartphone-based positioning on the Earth's surface. By multiplying the data recording interval and the number of samples accepted for calculation, the smoothing window used in GPS/EGNOS positioning can be obtained. A strictly defined minimum of uninterrupted epochs for smoothing the code pseudorange with carrier-phase observations is required for aeronautical applications based on [30]. Since we are not concerned with aeronautical positioning, for research purposes related to GPS/EGNOS positioning with a smartphone, several computational variants related to smoothing window and steady state were performed.

3. Results

Data associated with the Mi8 smartphone were recalculated in GPS/EGNOS mode according to [30], with the following variations: smoothing window—10 s, smoothing window—20 s, smoothing window—30 s, no smoothing.

Each of these options has sub-options: excluding satellites before reaching a steady state at 1 s, excluding satellites before reaching a steady state at 60 s, excluding satellites before reaching a steady state at 180 s, and excluding satellites before reaching steady state at 360 s.

Figures 2 and 3 show the results of the smoothing window and steady-state analysis of GPS/EGNOS positioning using an Mi8 smartphone compared to GPS/EGNOS positioning using a Septentrio AsteRx2 receiver. The horizontal positioning error (HPE) and vertical positioning error (VPE) values were calculated. Different colours indicate the number of individual solutions with similar values, so one can deduce which error values occurred most often in the calculations.

Already, using the results presented in Figure 2, we can deduce that for the Mi8 smartphone, the best accuracy obtained both horizontally and vertically is characterised by a steady state of 60 s and a smoothing window of 20 s. The numerical values of the accuracy analysis presented in Table 1 show that indeed, for both horizontal and vertical analysis, the best results of the mean positioning errors, their standard deviation, as well as the VPE_{\max} were obtained for a steady state of 60 s and a smoothing window of 20 ($HPE_{\text{mean}} = 2.24$ m, $HPE_{\text{std}} = 1.95$ m, $VPE_{\text{mean}} = 3.27$ m, $VPE_{\text{std}} = 2.78$ m, $VPE_{\max} = 24.48$). However, the best results of maximum horizontal error values were obtained for a steady state of 1 s and a smoothing window of 30 s, where $HPE_{\max} = 26.03$ m. In further analyses, a steady state of 60 s and a smoothing window of 20 s were assumed to be the best pairing among the analysed variants and were included in further analyses as a positioning variant using the Xiaomi Mi8 GPS/EGNOS smartphone.

In the case of the results obtained for the Septentrio AsteRx2 receiver presented in Figure 3, the differences obtained between the variants are not so noticeable, but the analysis of the numerical results obtained also identifies a steady state of 60 s and a smoothing window of 20 s as being optimal ($HPE_{\text{mean}} = 0.38$ m, $HPE_{\text{std}} = 0.17$ m, $HPE_{\max} = 1.48$ m, $VPE_{\text{mean}} = 0.50$ m, $VPE_{\text{std}} = 0.43$ m, $VPE_{\max} = 2.19$ m). Compared to the results obtained for the smartphone, this variant performs much better, which is understandable due to the different GNSS chipsets and antennas used in these two measuring devices.

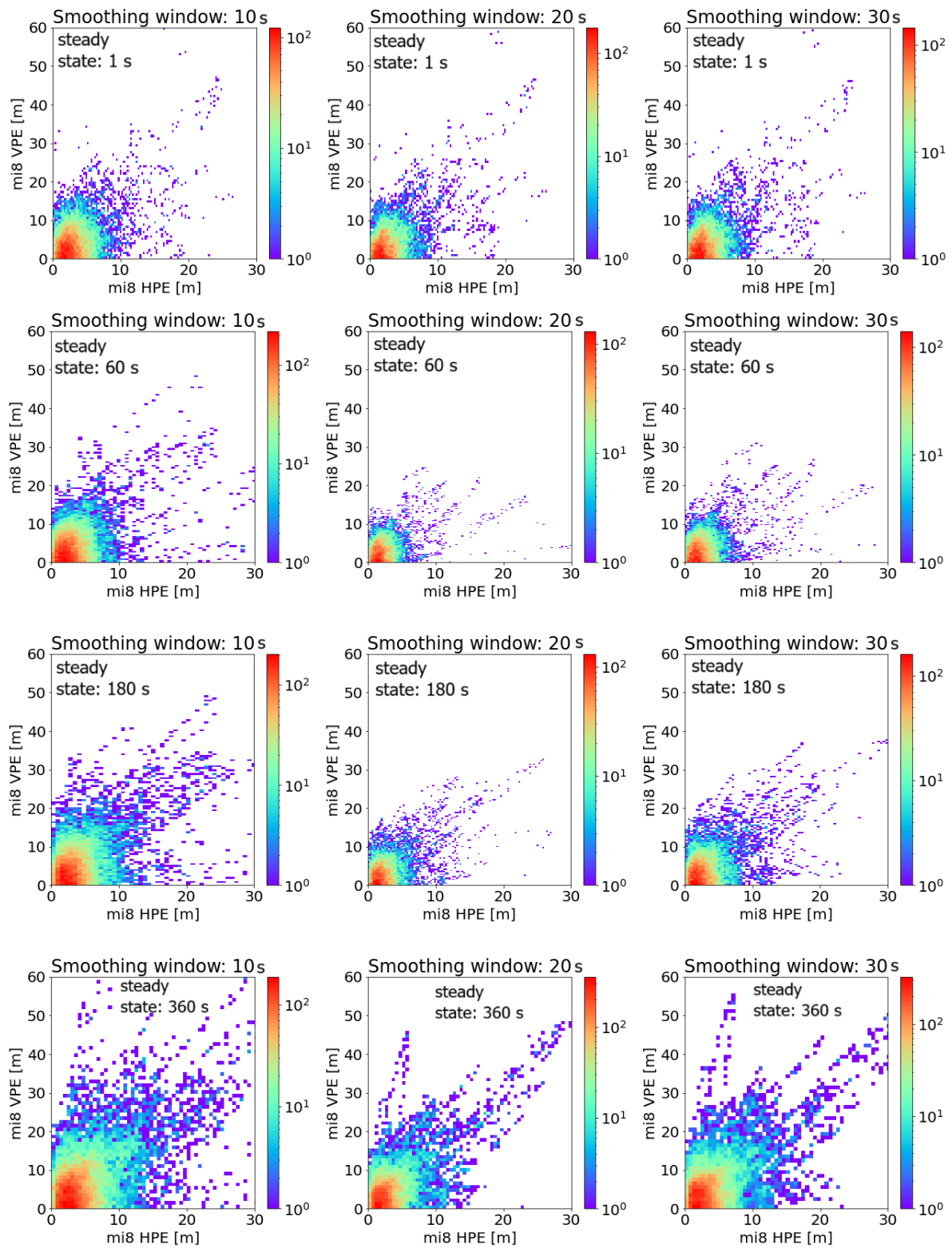


Figure 2. HPE and VPE values for Xiaomi Mi8 GPS/EGNOS steady-state smartphone positioning from top to bottom: 1 s, 60 s, 180 s, 360 s.

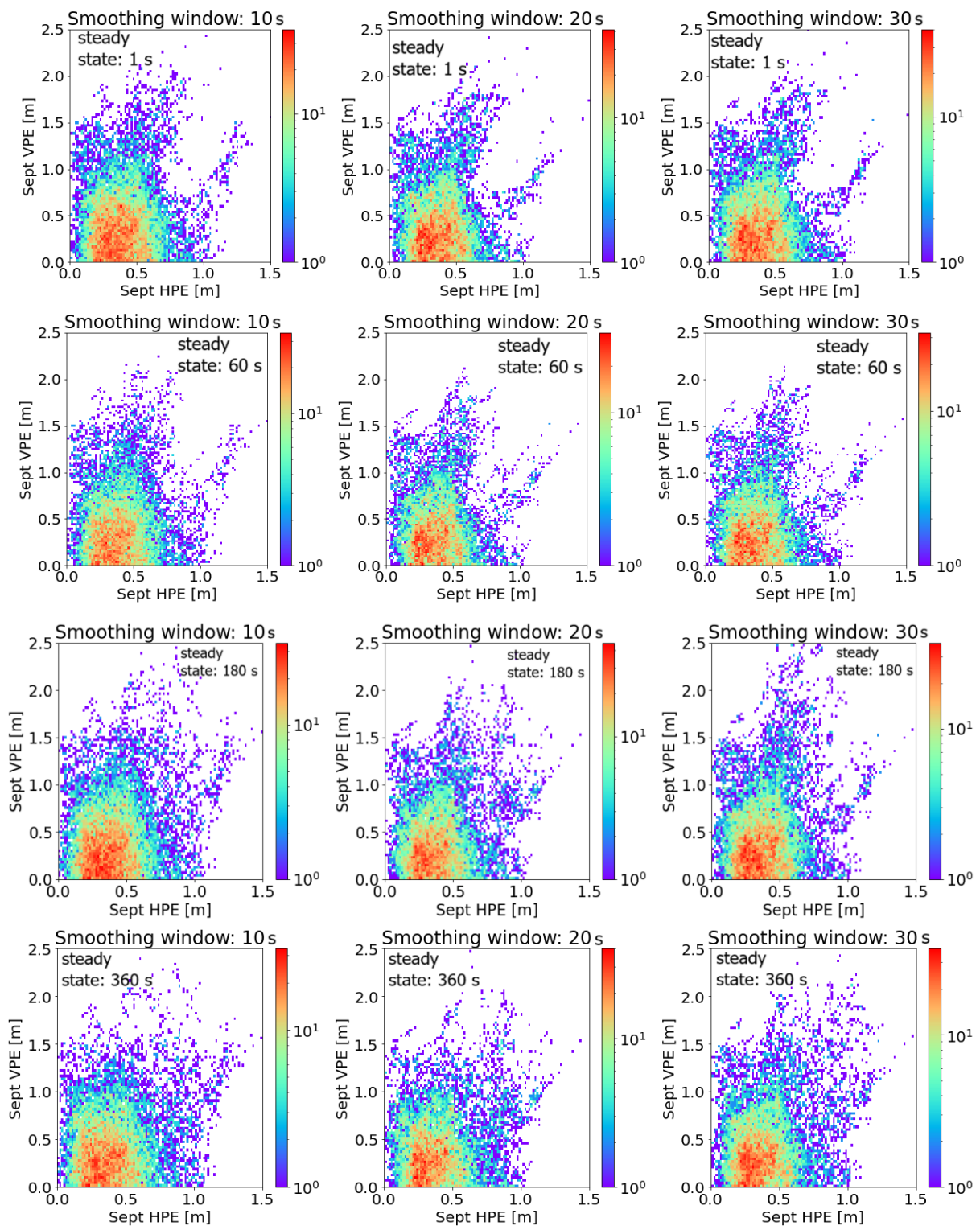


Figure 3. HPE and VPE values for Septentrio AsteRx2 GPS/EGNOS steady-state receiver positioning from top to bottom: 1 s, 60 s, 180 s, 360 s.

Table 1. Numerical values of the accuracy analysis performed for the Xiaomi Mi8 smartphone with varying steady states and smoothing windows.

Smoothing Window [s]	Steady State [s]	HPE _{mean} [m]	HPE _{std} [m]	HPE _{max} [m]	VPE _{mean} [m]	VPE _{std} [m]	VPE _{max} [m]
10	1	3.16	2.55	26.56	4.67	4.41	60.46
	60	3.23	2.85	57.05	4.52	4.22	48.37
	180	4.01	3.87	64.24	5.73	5.58	51.58
	360	4.74	5.42	86.87	22.21	46.78	171.00
20	1	2.84	2.46	26.25	4.25	4.23	59.31
	60	2.24	1.95	30.62	3.27	2.78	24.48
	180	3.12	2.84	40.65	4.47	4.27	39.29
	360	4.06	4.20	60.89	6.27	7.12	106.42
30	1	2.68	2.45	26.03	4.05	4.16	58.94
	60	2.59	2.22	33.49	3.70	3.25	30.84
	180	2.66	2.39	27.02	3.81	3.58	32.71
	360	3.48	3.66	50.00	5.41	6.21	86.42
No smoothing	-	4.47	3.01	43.04	6.38	5.32	64.95

Figure 4 compares the best GPS/EGNOS positioning result with smoothing (steady state of 60 s and a smoothing window of 20 s) with the solution without smoothing code observations. It can be seen that the vertical and horizontal accuracy results are significantly better for the solution based on smoothing (according to Table 1: for the no-smoothing variant, HPE_{mean} = 4.47 m, HPE_{std} = 3.01 m, HPE_{max} = 43.03 m, VPE_{mean} = 6.38 m, VPE_{std} = 5.32 m, VPE_{max} = 64.95 m). Also noticeable in Figure 4 is the significant improvement in vertical positioning accuracy when using carrier-phase smoothed code observation. In the case of the analysis performed for the Septentrio AsteRx2 receiver, similar conclusions were also drawn (for the no-smoothing variant, HPE_{mean} = 0.44 m, HPE_{std} = 0.23 m, HPE_{max} = 1.89 m, VPE_{mean} = 0.58 m, VPE_{std} = 0.50 m, VPE_{max} = 3.77 m).

The next stage of the research was to analyse the use of different observation weighting strategies in the observation model. The Xiaomi Mi 8 device is equipped with a Broadcom chipset, BCM4775, GLL ver. 107.20.22 414037, characterised by dual-frequency (E1/L1 + E5/L5) satellite observation capabilities. The quality of GNSS positioning using smartphones is highly dependent on the antenna design these devices are equipped with [26,41–43]. Smartphone GNSS antennas are characterised by low gain and low multipath resistance [44,45]. As a rule, mobile devices are equipped with either omnidirectional linearly or elliptically polarised antennas due to the theoretically differently oriented smartphone performing the positioning [46].

When using more advanced GNSS receivers and their antennas, the signal-to-noise ratio increases with increasing elevation, whereas this relationship cannot be observed for smartphone devices [47]. Therefore, for calculations related to data acquired with a smartphone, a signal-to-noise ratio-dependent weighting model is preferred to one related to satellite elevation [48].

The study analysed the impact of the type of observation weighting within the autonomous positioning model using a Xiaomi Mi8 smartphone (Formula (14)). Values of standard deviation are equal to 1 ($\sigma = 1$), dependent on satellite elevation and dependent on the value of the signal-to-noise ratio.

$$W = \frac{1}{\sigma^2} \quad (14)$$

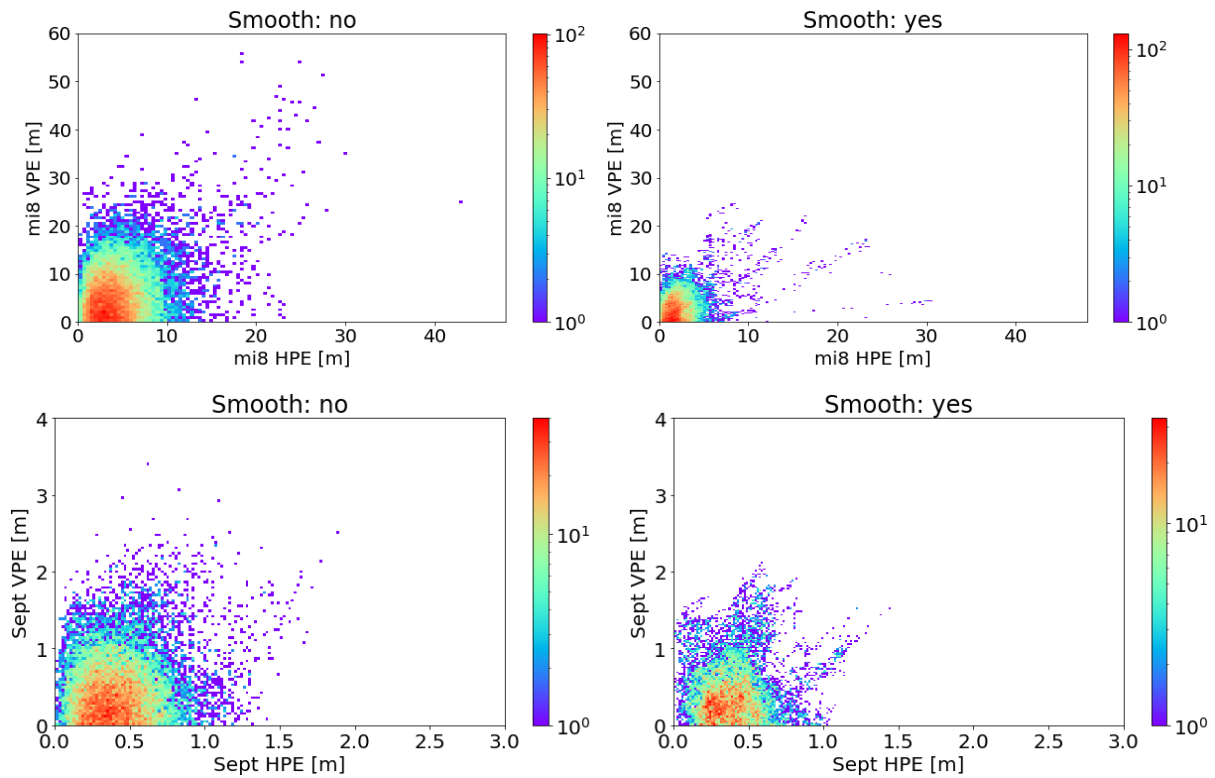


Figure 4. HPE and VPE values for GPS/EGNOS positioning with a steady state of 60 s and a smoothing window of 20s versus GPS/EGNOS with no smoothing (upper figures—Xiaomi Mi8, lower figures—Septentrio AsteRx2).

In the case of the option of adopting a satellite elevation-dependent standard deviation value, it takes the following form:

$$\sigma = a + b \cdot e^{(-E/c)} \tag{15}$$

where

E is the satellite elevation.

According to [30], $a = 0.13$ m, $b = 0.53$ m, $c = 10^\circ$.

A variant taking the value of the standard deviation depending on the signal-to-noise ratio's standard deviation takes the following form:

$$\sigma = a + b \cdot 10^{(-SNR/10)} \tag{16}$$

where

SNR is the signal-to-noise ratio for pseudorange measurement.

In the case of positioning using SBAS systems, according to [30], the calculation associated with the σ takes the following form:

$$\sigma_i^2 = \sigma_{i,flt}^2 + \sigma_{i,UIRE}^2 + \sigma_{i,air}^2 + \sigma_{i,tropo}^2 \tag{17}$$

where

σ_i^2 is the variance of pseudorange measurement;

$\sigma_{i,flt}^2$ is the variance of rapid and long-term adjustments;

$\sigma_{i,UIRE}^2$ is the ionospheric delay variance;

$\sigma_{i,air}^2$ is the variance associated with the operation of the GNSS receiver;

$\sigma_{i,tropo}^2$ is the tropospheric delay variance.

Figure 5 shows the SNR (signal-to-noise ratio) and elevation values of sample satellites associated with observations acquired with a Xiaomi Mi8 smartphone and a Septentrio AsteRx2 receiver. For the Mi8 smartphone, it can be seen that there is no correlation between satellite elevation and SNR, which cannot be inferred for the data presented for the AsteRx2 receiver. The impact of SNR on smartphone positioning is considered in further analyses related to autonomous positioning and GPS/EGNOS.

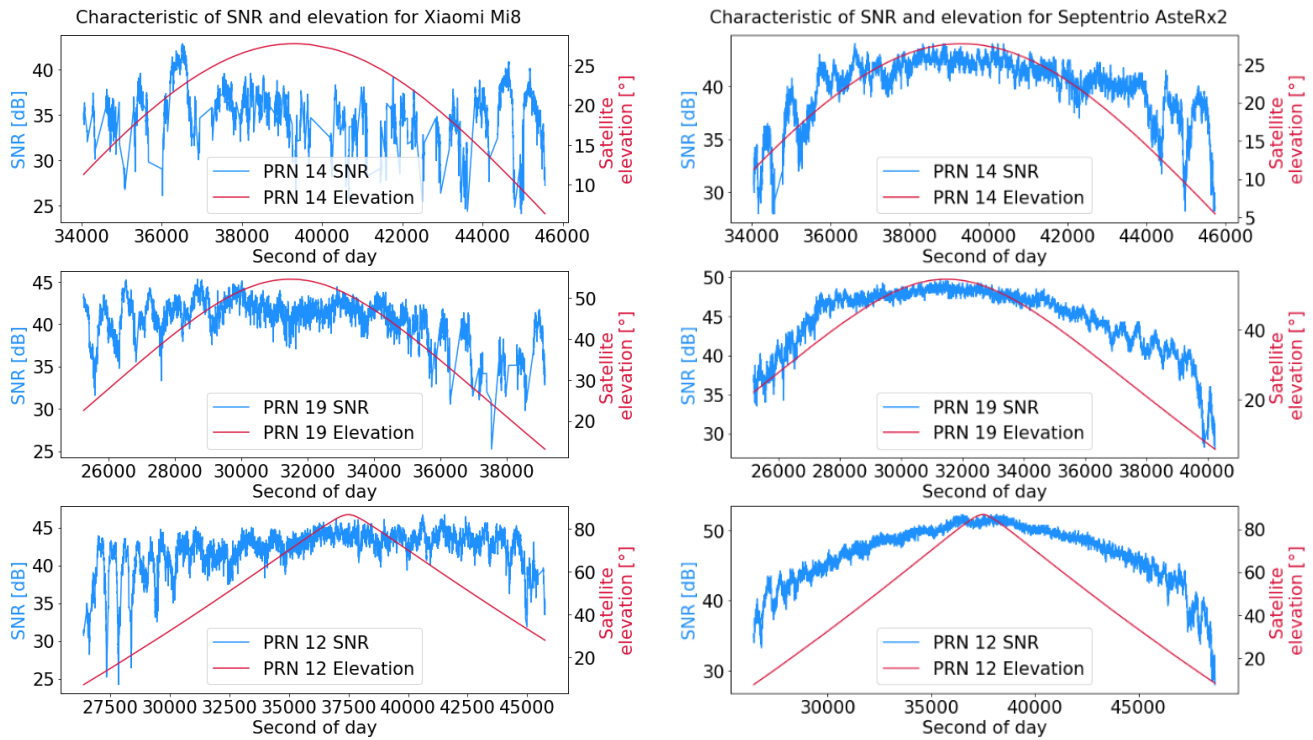


Figure 5. SNR and elevation of example satellites observed during measurements with a Xiaomi Mi8 and Septentrio AsteRx2.

Figure 6 shows the results of autonomous positioning smoothed by phase observations in post-processing mode using a Xiaomi Mi8 smartphone and a Septentrio AsteRx2 receiver and considering different variants of observation weighting (i.e., weight equal to 1, weight dependent on satellite elevation, and weight dependent on SNR). For the Mi8 smartphone and the variant weighting equal to 1, the results were $HPE_{\text{mean}} = 3.22$ m, $HPE_{\text{std}} = 2.66$ m, $HPE_{\text{max}} = 55.08$ m, $VPE_{\text{mean}} = 4.39$ m, $VPE_{\text{std}} = 4.29$ m, and $VPE_{\text{max}} = 123.29$ m. The variant taking the weighting of observations according to SNR for the Mi8 smartphone presents the best results in this analysis: $HPE_{\text{mean}} = 2.72$ m, $HPE_{\text{std}} = 2.18$ m, $HPE_{\text{max}} = 53.56$ m, $VPE_{\text{mean}} = 3.90$ m, $VPE_{\text{std}} = 3.82$ m, and $VPE_{\text{max}} = 88.14$ m. In contrast, in the case of the Mi8 smartphone, the variant for the observation weight depending on the satellite elevation gave worse results: $HPE_{\text{mean}} = 4.70$ m, $HPE_{\text{std}} = 3.72$ m, $HPE_{\text{max}} = 69.07$ m, $VPE_{\text{mean}} = 6.58$ m, $VPE_{\text{std}} = 5.63$ m, and $VPE_{\text{max}} = 96.68$ m. For the Septentrio AsteRx2 receiver, the results of various variants are not as significantly different. The smallest maximum error of horizontal and vertical positioning was obtained for the variant based on the weight depending on the elevation of the satellite ($HPE_{\text{max}} = 2.44$ m, $VPE_{\text{max}} = 4.35$ m). On the other hand, variants based on weighting equal to 1 and dependent on SNR obtained the best results for HPE_{mean} , VPE_{mean} , HPE_{std} , and VPE_{std} (see Table 2).

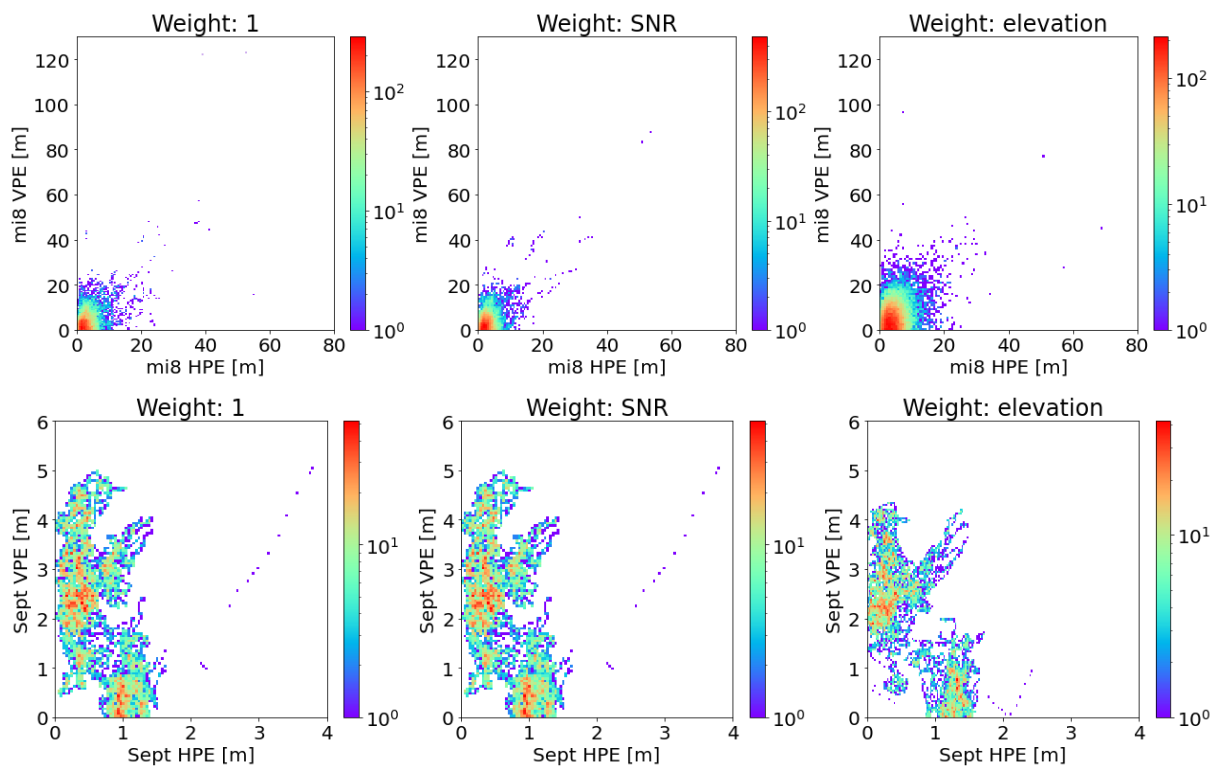


Figure 6. HPE and VPE values for GPS autonomous positioning smoothed with carrier-phase observations for a smoothing window of 20 s with different variants of observation weighting (upper figures—Xiaomi Mi8, lower figures—Septentrio AsteRx2).

Table 2. Numerical values of the accuracy analysis performed for GPS autonomous positioning with carrier-phase smoothed code observations for the Xiaomi Mi8 smartphone and the Septentrio AsteRx2 receiver with different variants of observation weighting. All values are expressed in meters.

Receiver	Weighting Variant	HPE _{mean}	HPE _{std}	HPE _{max}	VPE _{mean}	VPE _{std}	VPE _{max}
Xiaomi Mi8	1	3.22	2.66	55.08	4.39	4.29	123.29
	SNR	2.72	2.18	53.56	3.90	3.82	88.14
	elevation	4.70	3.72	69.08	6.58	5.63	96.68
Septentrio AsteRx2	1	0.64	0.37	3.81	2.20	1.26	5.06
	SNR	0.62	0.37	3.81	2.15	1.29	5.06
	elevation	0.66	0.47	2.44	2.07	1.11	4.35

4. Discussion

Table 3 summarises the results of the accuracy analysis for three positioning variants with the Xiaomi Mi8 smartphone: autonomous GPS (SNR-dependent observation weighting); GPS/EGNOS with a smoothing window of 20 and steady state of 60 s (SNR-dependent observation weighting); and GPS/EGNOS with a smoothing window of 20 s and a steady state of 60 s (standard EGNOS weighting model). The results clarify that the GPS/EGNOS variant with the EGNOS weighting model presents the best accuracy, which may indicate a fairly good adaptation of the component observation weights to the performance of the Mi8 smartphone positioning model. Also noteworthy are the vertical results, which have a lower maximum error than the horizontal analysis. The GSP/EGNOS variant with the standard weighting model obtained the following results: HPE_{mean} = 2.24 m, HPE_{std} = 1.95 m, HPE_{max} = 30.62 m, VPE_{mean} = 3.27 m, VPE_{std} = 2.78 m, and VPE_{max} = 24.48 m.

Table 3. Numerical values of the accuracy analysis performed for positioning with the Xiaomi Mi8 smartphone: autonomous GPS (SNR-dependent observation weighting); GPS/EGNOS with a smoothing window of 20 s and a steady state of 60 s (SNR-dependent observation weighting); and GPS/EGNOS with a smoothing window of 20 s and a steady state of 60 s (standard EGNOS weighting model). All values are expressed in meters.

Receiver	Positioning Variant	HPE _{mean}	HPE _{std}	HPE _{max}	VPE _{mean}	VPE _{std}	VPE _{max}
Xiaomi Mi8	GPS autonomous (weight: SNR)	2.72	2.18	53.56	3.90	3.82	88.14
	GPS/EGNOS, smoothing window: 20 s; steady state: 60 s (weight: SNR)	2.59	2.24	33.26	3.65	3.25	30.83
	GPS/EGNOS, smoothing window: 20 s; steady state: 60 s (standard EGNOS weighting model)	2.24	1.95	30.62	3.27	2.78	24.48

The final part of the study analyses the possibility of manipulating the components of the pseudorange correction that is applied in the GPS/EGNOS positioning algorithm. This analysis aims to test the feasibility of reducing the amount of correction data applied to the smartphone, which is necessary to achieve accuracy close to the GPS/EGNOS variant. Figure 7 and Table 4 show that horizontally, the variants with RRC (range rate correction) off and Iono correction off perform well, while vertically, only the variant with RRC off produces good results. It is noteworthy that the lack of ionospheric correction has a significant impact on the mean vertical accuracy and standard deviation (VPE_{mean} = 5.00 m, VPE_{std} = 3.69 m). The largest maximum vertical positioning error is presented by the slow-correction-off variant (VPE_{max} = 39.03). For the horizontal analysis, the slow-correction-off variant (HPE_{mean} = 3.09 m, HPE_{std} = 2.57 m, HPE_{max} = 43.93 m) was unequivocally the worst. For the Septentrio receiver, it is clear that the RRC-off variant is characterised by results close to the original EGNOS solution (HPE_{mean} = 0.39 m, HPE_{std} = 0.18 m, HPE_{max} = 1.24 m, VPE_{mean} = 0.45 m, VPE_{std} = 0.36 m, VPE_{max} = 1.97 m). For both the Mi8 smartphone and the Septentrio receiver, the SNR-dependent weighting variant performs moderately well for both horizontal and vertical positioning.

Table 4. Numerical values of the accuracy analysis performed for GPS/EGNOS positioning with a Xiaomi Mi8 smartphone and Septentrio AsteRx2 receiver in different variants. All values are expressed in meters.

Receiver	Variant	HPE _{mean}	HPE _{std}	HPE _{max}	VPE _{mean}	VPE _{std}	VPE _{max}
Xiaomi Mi8	W: SNR	2.59	2.24	33.26	3.65	3.25	30.83
	Original EGNOS	2.24	1.95	30.62	3.27	2.78	24.48
	Iono correction off	2.64	2.25	30.68	5.00	3.69	32.10
	Fast correction off	2.80	2.31	32.88	4.18	3.54	30.51
	Slow correction off	3.09	2.57	43.93	3.66	3.29	39.03
	RRC off	2.59	2.22	33.49	3.70	3.25	30.84
	Fast and slow correction off	2.80	2.45	38.97	3.73	3.35	38.70
	Fast, RRC, slow correction off	2.80	2.45	38.97	3.73	3.35	38.70
Septentrio AsteRx2	IN: SNR	0.62	0.37	3.81	2.15	1.29	5.06
	Original EGNOS	0.39	0.18	1.48	0.45	0.36	2.13
	Iono correction off	0.73	0.26	1.70	2.87	0.67	5.25
	Fast correction off	1.30	0.61	3.53	1.12	0.76	3.47
	Slow correction off	1.17	0.44	2.50	1.43	0.76	4.09
	RRC off	0.39	0.18	1.24	0.45	0.36	1.97
	Fast and slow correction off	0.74	0.42	1.81	0.73	0.56	2.37
	Fast, RRC, slow correction off	0.74	0.42	1.81	0.73	0.56	2.37

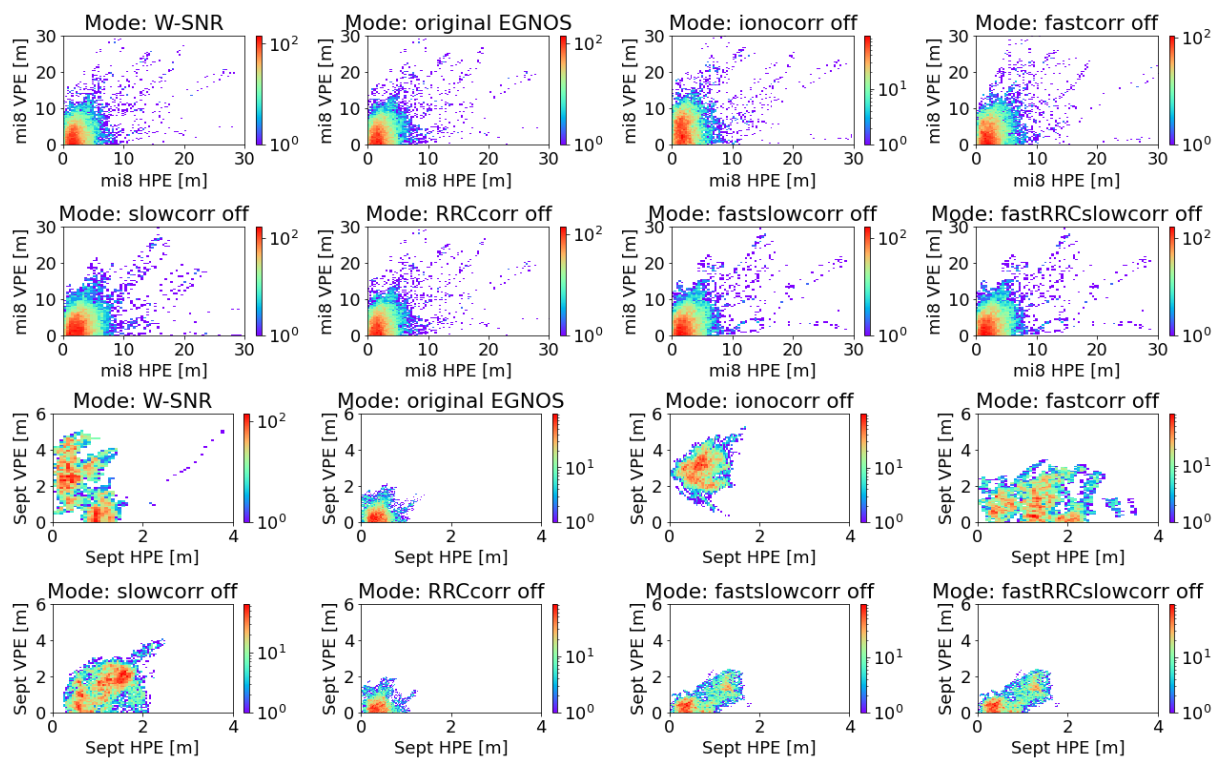


Figure 7. HPE and VPE values for GPS/EGNOS positioning smoothed with carrier-phase observations using a smoothing window of 20 s with different variants of pseudorange correction components (upper figures—Xiaomi Mi8, lower figures—Septentrio AsteRx2).

5. Conclusions

The intention of the analyses presented here was to indicate possible modifications to the standard GPS/EGNOS algorithm, with a view to using it in its most optimal form in smartphone-type mobile devices. The results obtained indicate the use of steady-state values other than those recommended for aeronautical purposes related to the smoothing of observations. The smoothing of code observations alone for mobile devices has a positive impact on the quality of positioning. For autonomous positioning, the signal-to-noise-related weighting model gives better accuracy results than the satellite elevation-related observation weighting model. However, in the case of positioning using SBAS data, the EGNOS weighting model performs best. Interfering with the components of the corrections to the pseudorange indicated that in order to process fewer data, it is possible to dispense with range rate corrections without degrading positioning accuracy. In the case of vertical positioning, the use of ionospheric corrections is of great importance for accuracy.

Author Contributions: Conceptualization, G.G. and A.C.; Data curation, D.T.; Formal analysis, K.K.; Funding acquisition, G.G.; Investigation, G.G.; Methodology, G.G.; Project administration, G.G.; Resources, G.G.; Software, G.G.; Supervision, K.K.; Validation, A.C.; Visualization, D.T.; Writing—original draft, G.G.; Writing—review and editing, A.C. All authors have read and agreed to the published version of the manuscript.

Funding: This research was funded by the University of Warmia and Mazury in Olsztyn.

Institutional Review Board Statement: Not applicable.

Informed Consent Statement: Not applicable.

Data Availability Statement: The data presented in this study are available on request from the corresponding author.

Conflicts of Interest: Author Dariusz Tanajewski was employed by the company Four Point. The remaining authors declare that the research was conducted in the absence of any commercial or financial relationships that could be construed as a potential conflict of interest.

References

1. Park, K.W.; Park, J.-I.; Park, C. Efficient methods of utilizing multi-SBAS corrections in multi-GNSS positioning. *Sensors* **2020**, *20*, 256. [CrossRef]
2. Krzykowska-Piotrowska, K.; Dudek, E.; Wielgosz, P.; Milanowska, B.; Batalla, J.M. On the Correlation of Solar Activity and Troposphere on the GNSS/EGNOS Integrity. A Fuzzy Logic Approach. *Energies* **2021**, *14*, 4534. [CrossRef]
3. Kahlouche, S.; Benadda, B. Performance of the EGNOS system in Algeria for single and dual frequency. *Int. J. Aviat. Aeronaut. Aerosp.* **2021**, *8*, 8.
4. Kahlouche, S. Assessment of EGNOS performance for civil aviation flight phase in the edge coverage area. *Int. J. Aviat. Aeronaut. Aerosp.* **2020**, *7*, 1.
5. Barrios, J.; Pericacho, J.G.; Arenas, J.; Liu, J.X.; Domenech, S.; Bernárdez, J.M.; Bunce, D. Lessons Learned from SBAS Systems and Testbeds for the Global SBAS Concept. In Proceedings of the 34th International Technical Meeting of the Satellite Division of the Institute of Navigation (ION GNSS+ 2021), St. Louis, MI, USA, 20–24 September 2021; pp. 1516–1549.
6. Specht, M. Consistency of the empirical distributions of navigation positioning system errors with theoretical distributions—comparative analysis of the DGPS and EGNOS systems in the years 2006 and 2014. *Sensors* **2021**, *21*, 31. [CrossRef]
7. Ibáñez Segura, D.; Rovira Garcia, A.; Alonso, M.T.; Sanz, J.; Juan, J.M.; Gonzalez Casado, G.; López Martínez, M. EGNOS 1046 Maritime Service Assessment. *Sensors* **2020**, *20*, 276. [CrossRef]
8. Flament, D.; Thomas, D.; Lopez, C.; Melinotte, J.M.; Urbanska, K.; Derambure, X.; Boisseau, A. EGNOS System Evolutions in Europe and within the International Multi-SBAS context. In Proceedings of the 2020 European Navigation Conference (ENC), Dresden, Germany, 23–24 November 2020; IEEE: New York, NY, USA, 2020; pp. 1–13.
9. Yayla, G.; Van Baelen, S.; Peeters, G.; Afzal, M.R.; Singh, Y.; Slaets, P. Accuracy benchmark of Galileo and EGNOS for Inland Waterways. In Proceedings of the International Ship Control Systems Symposium (iSCSS), Online, 6–8 October 2020; pp. 1–10.
10. Alarcón, F.; Viguria, A.; Vilardaga, S.; Montolio, J.; Soley, S. EGNOS-based Navigation and Surveillance System to Support the Approval of RPAS Operations. In Proceedings of the 9th SESAR Innovation Days, Athens, Greece, 2–5 December 2019; pp. 2–6.
11. Zangenehjad, F.; Gao, Y. GNSS smartphone positioning: Advances, challenges, opportunities, and future perspectives. *Satell. Navig.* **2021**, *2*, 24. [CrossRef]
12. Gogoi, N.; Minetto, A.; Linty, N.; Dovic, F. A controlled-environment quality assessment of android GNSS raw measurements. *Electronics* **2019**, *8*, 5. [CrossRef]
13. European Global Navigation Satellite Systems Agency (GSA). Worlds First Dual-Frequency GNSS Smartphone Hits the Market. Available online: <https://www.gsa.europa.eu/newsroom/news/world-s-first-dual-frequency-gnss-smartphone-hits-market> (accessed on 17 August 2021).
14. Massarweh, L.; Darugna, F.; Psychas, D.; Bruno, J. Statistical investigation of android GNSS data: Case study using Xiaomi Mi 8 dual-frequency raw measurements. In Proceedings of the 32nd International Technical Meeting of the Satellite Division of the Institute of Navigation (ION GNSS+ 2019), Miami, FL, USA, 16–20 September 2019; pp. 3847–3861.
15. Paziewski, J.; Fortunato, M.; Mazzoni, A.; Odolinski, R. An analysis of multi-GNSS observations tracked by recent Android smartphones and smartphone-only relative positioning results. *Measurement* **2021**, *175*, 109162. [CrossRef]
16. Fortunato, M.; Ravanelli, M.; Mazzoni, A. Real-time geophysical applications with Android GNSS raw measurements. *Remote Sens.* **2019**, *11*, 2113. [CrossRef]
17. Psychas, D.; Bruno, J.; Massarweh, L.; Darugna, F. Towards sub-meter positioning using Android raw GNSS measurements. In Proceedings of the 32nd International Technical Meeting of the Satellite Division of the Institute of Navigation (ION GNSS+ 2019), Miami, FL, USA, 16–20 September 2019; pp. 3917–3931.
18. Gao, R.; Xu, L.; Zhang, B.; Liu, T. Raw GNSS observations from Android smartphones: Characteristics and short-baseline RTK positioning performance. *Meas. Sci. Technol.* **2021**, *32*, 084012. [CrossRef]
19. Miralles, D.; Levigne, N.; Akos, D.M.; Blanch, J.; Lo, S. Android raw GNSS measurements as the new anti-spoofing and anti-jamming solution. In Proceedings of the 31st International Technical Meeting of the Satellite Division of the Institute of Navigation (ION GNSS+ 2018), Miami, FL, USA, 24–28 September 2018; pp. 334–344.
20. Robustelli, U.; Baiocchi, V.; Pugliano, G. Assessment of dual frequency GNSS observations from a Xiaomi Mi 8 Android smartphone and positioning performance analysis. *Electronics* **2019**, *8*, 91. [CrossRef]
21. Robustelli, U.; Paziewski, J.; Pugliano, G. Observation quality assessment and performance of GNSS standalone positioning with code pseudoranges of dual-frequency Android smartphones. *Sensors* **2021**, *21*, 2125. [CrossRef]
22. Weng, D.; Gan, X.; Chen, W.; Ji, S.; Lu, Y. A new DGNS positioning infrastructure for android smartphones. *Sensors* **2020**, *20*, 487. [CrossRef]
23. Morán, J.; Vázquez, J.; Sánchez, M.A.; Pampanas, H.; González, J.R. Enhancing Smartphones' Location with EDAS (EGNOS Data Access Service) Internet Corrections. In Proceedings of the 33rd International Technical Meeting of the Satellite Division of the Institute of Navigation (ION GNSS+ 2020), Online, 21–25 September 2020; pp. 1821–1836.

24. Lim, C.; Shin, D.; Park, B.; Kee, C.; Seo, S.; Park, J.; Cho, A. L1 SFMC SBAS System to Improve the Position Accuracy of Android Device. In Proceedings of the 31st International Technical Meeting of the Satellite Division of the Institute of Navigation (ION GNSS+ 2018), Miami, FL, USA, 24–28 September 2018; pp. 455–481.
25. Shao, B.; Ding, Q.; Wu, X. Estimation method of SBAS dual-frequency range error integrity parameter. *Satell. Navig.* **2020**, *1*, 9. [[CrossRef](#)]
26. Joly, D.; de Echazarreta, C.L. EGNOS High Integrity System Test Bed (HISTB): A First Implementation of Dual Frequencies Multi Constellations Standard. In Proceedings of the 31st International Technical Meeting of the Satellite Division of the Institute of Navigation (ION GNSS+ 2018), Miami, FL, USA, 24–28 September 2018; pp. 2134–2141.
27. Salos, D.; Mabileau, M.; Rodriguez, C.; Secretan, H.; Suard, N.; Dufour, F.; Estival, P. SBAS DFMC Analysis with a Software Prototype. In Proceedings of the 30th International Technical Meeting of the Satellite Division of the Institute of Navigation (ION GNSS+ 2017), Portland, Oregon, 25–29 September 2017; pp. 2019–2030.
28. Tabti, L.; Kahlouche, S.; Chikouche, D.; Benadda, B. Improvement of single-frequency GPS positioning performance based on EGNOS corrections in Algeria. *J. Navig.* **2020**, *73*, 846–860. [[CrossRef](#)]
29. International Civil Aviation Organization (ICAO). *PEGASUS*; Technical Notes on SBAS, DocNo: PEG-TN-SBAS; ICAO: Montreal, QC, Canada, 2023.
30. RTCA DO-229; Minimum Operational Performance Standards for Airborne Equipment Using Global Positioning System/Wide Area Augmentation System. Radio Technical Committee for Aeronautics: Washington, DC, USA, 2013.
31. Grunwald, G.; Bakula, M.; Ciecko, A.; Kazmierczak, R. Examination of GPS/EGNOS integrity in north-eastern Poland. *IET Radar Sonar Navig.* **2016**, *10*, 114–121. [[CrossRef](#)]
32. Ciecko, A. Analysis of the EGNOS quality parameters during high ionosphere activity. *IET Radar Sonar Navig.* **2019**, *13*, 1131–1139. [[CrossRef](#)]
33. Ciecko, A.; Grunwald, G. Klobuchar, NeQuick G, and EGNOS Ionospheric Models for GPS/EGNOS Single-Frequency Positioning under 6–12 September 2017 Space Weather Events. *Appl. Sci.* **2020**, *10*, 1553. [[CrossRef](#)]
34. Shan, W.; Ding, W.; Yingxuan, G. An Improved Ionospheric Delay Correction Method for SBAS. *Chin. J. Electron.* **2021**, *30*, 384–389. [[CrossRef](#)]
35. Arenas, J.; Rovira-Garcia, A.; Juan, J.M.; Sanz, J.; Gonzalez-Casado, G.; Ibañez, D.; Orus, R. Low-latitude ionospheric effects on SBAS. *Radio. Sci.* **2016**, *51*, 603–618. [[CrossRef](#)]
36. Zhigang, G.; Shuliang, L.; Rui, H. Estimation of Ionospheric Differential Corrections of Navigation Signals with Kalman Filter. *Geomatics Inf. Sci. Wuhan Univ.* **2010**, *9*, 1021–1023.
37. Kos, T.; Botincan, M.; Markezic, I. Evaluation of EGNOS tropospheric delay model in south-eastern Europe. *J. Navig.* **2009**, *62*, 341–349. [[CrossRef](#)]
38. Zhang, X.; Huang, P. Optimal Hatch Filter with an adaptive smoothing time based on SBAS. In Proceedings of the 2nd International Conference on Soft Computing in Information Communication Technology, Taipei, Taiwan, 31 May–1 June 2014; pp. 34–38.
39. Ibañez, D.; Rovira-García, A.; Sanz, J.; Juan, J.M.; Gonzalez-Casado, G.; Jimenez-Baños, D.; López-Echazarreta, C.; Lapin, I. The GNSS Laboratory Tool Suite (gLAB) updates: SBAS, DGNSS and Global Monitoring System. In Proceedings of the 9th ESA Workshop on Satellite Navigation Technologies (NAVITEC 2018), Noordwijk, The Netherlands, 5–7 December 2018. [[CrossRef](#)]
40. Geomatics, Navigation and Positioning Lab, UPC. GLAB Tool Suite. Geomatics Engineering Area UPC. Available online: <https://gage.upc.edu/en/learning-materials/software-tools/glab-tool-suite> (accessed on 5 January 2024).
41. Gioia, C.; Borio, D. NeQuick-G and Android Devices: A Compromise between Computational Burden and Accuracy. *Sensors* **2020**, *20*, 5908. [[CrossRef](#)]
42. Riley, S.; Lentz, W.; Clare, A. On the path to precision-observations with android GNSS observables. In Proceedings of the 30th International Technical Meeting of the Satellite Division of the Institute of Navigation (ION GNSS+ 2017), Portland, Oregon, 25–29 September 2017; pp. 116–129.
43. Chen, B.; Li, Z.; Zhang, Q.; Li, X.; Yu, C.; El-Sheimy, N. Real-time precise point positioning with a Xiaomi MI 8 android smartphone. *Sensors* **2019**, *19*, 2835. [[CrossRef](#)]
44. Geng, J.; Li, G. On the feasibility of resolving Android GNSS carrier-phase ambiguities. *J. Geod.* **2019**, *93*, 2621–2635. [[CrossRef](#)]
45. Lachapelle, G.; Gratton, P.; Horrejt, J.; Lemieux, E.; Broumandan, A. Evaluation of a low cost hand held unit with GNSS raw data capability and comparison with an android smartphone. *Sensors* **2018**, *18*, 4185. [[CrossRef](#)] [[PubMed](#)]
46. Inside GNSS. Smartphone-Based GNSS Positioning: Today and Tomorrow. Available online: <https://insidegnss.com/smartphone-based-gnss-positioning-today-and-tomorrow/> (accessed on 10 October 2023).
47. Zhu, H.; Xia, L.; Wu, D.; Xia, J.; Li, Q. Study on Multi-GNSS Precise Point Positioning Performance with Adverse Effects of Satellite Signals on Android Smartphone. *Sensors* **2020**, *20*, 6447. [[CrossRef](#)]
48. Zhang, X.; Li, Z.; Guo, F.; Ren, X.; Zhang, K.; He, X. Quality assessment of GNSS observations from an Android N smartphone and positioning performance analysis using time-differenced filtering approach. *GPS Solut.* **2018**, *22*, 70. [[CrossRef](#)]

Disclaimer/Publisher’s Note: The statements, opinions and data contained in all publications are solely those of the individual author(s) and contributor(s) and not of MDPI and/or the editor(s). MDPI and/or the editor(s) disclaim responsibility for any injury to people or property resulting from any ideas, methods, instructions or products referred to in the content.